CHEMSUSCHEM

ChemPubSoc Europe

DOI: 10.1002/cssc.201200016

A Light-Assisted Biomass Fuel Cell for Renewable Electricity Generation from Wastewater

Rachel L. Chamousis and Frank E. Osterloh*[a]

A solar-energy-driven biomass fuel cell for the production of electricity from wastewater using only air and light as additional resources is described. The device consists of a photoelectrochemical cell that contains a nanostructured titanium dioxide or tungsten trioxide film as photoanode and a platinum air electrode as cathode, in separate compartments. The TiO_2 or WO_3 films are fabricated from TiO_2 nanocrystals or from sodium tungstate solutions on top of fluorine-doped tin dioxide. Devices were tested with electrolyte only, synthetic wastewater, or with aqueous glucose solution, under irradiation with sunlight, broad spectral illumination, and monochromatic light. Measured light conversion efficiencies were between 0.007% and 1.7%, depending on conditions. The highest efficiency (1.7%) and power output (0.73 $mW\,cm^{-2}$) are determined for TiO_2 electrodes under 395 nm illumination. In contrast to TiO_2, the WO_3 electrodes are active under visible light (>440 nm), but the IPCE value is low (2%). Apart from limited visible-light absorption, the overall performance of the device is limited by the substrate concentration in the water and by transport resistance through the cell.

Introduction

Treatment of municipal wastewater in the US consumes $25 billion annually and a significant fraction of the US energy.[1] Recently, microbial fuel cells (MFCs) that can degrade biomass in wastewater (glucose, fats, proteins, ammonia) into electricity using electrodes coated with biofilms of electroactive bacteria have been described.[1a,2] However, the power output and efficiency of the MFCs is low (0.25 $mW\,cm^{-2}$) and the bacteria are easily deactivated by contaminants in the wastewater. A potential alternative to this technology consists in the use of a photoelectrochemical cell (PEC), where an illuminated semiconductor electrode drives electrochemical reactions in the solution phase (Figure 1 A). Typically, PECs are classified either as regenerative cells that convert solar energy into electricity[3] or as fuel-producing cells that generate hydrogen via the water-splitting reaction.[4] In 1976, Bard et al. described a regenerative PEC that combined a TiO_2 photoelectrode with a platinum air electrode.[5] This cell oxidized water to oxygen at the photoanode and reduced oxygen to water at the platinum cathode. The performance of the cell was limited by the low visible light absorption of TiO_2 and by the water oxidation and oxygen reduction overpotentials. The hypothesis for the work described herein is that the power output of the Bard PEC can be raised by replacing the water in the cell with a solution of oxidizable biomass, as it occurs in municipal wastewater. Under these altered conditions, the photogenerated holes in the semiconductor then oxidize the biomass in the electrolyte to carbon dioxide, and the electrons are funneled to the platinum counterelectrode, where they reduce oxygen from air to water. This is shown in the energy diagram in Figure 1 A. The balanced chemical equation for this reaction is presented in Equation (1). Thus, the PEC would perform as a "light-assisted biomass fuel cell" that converts biomass into electricity, with only sunlight and air required as additional resources.

$$(HCOH)_n + n\,O_2 \xrightarrow{PEC,\,h\nu} n\,CO_2 + n\,H_2O \quad (1)$$

The energy efficiency of such a device can be estimated through the ratio of electrical power output (P_{Out}) and photochemical energy input ($P_{h\nu}$), as shown in Equation (2).

$$\eta = \frac{P_{Out}}{P_{In}} = \frac{V_{OC} I_{SC} FF}{P_{h\nu} + \frac{dn}{dt}\Delta G^0_{Ox}} \quad (2)$$

Herein, V_{OC}, I_{SC}, and FF are the open-circuit voltage, short-circuit current density, and fill factor, respectively. The term ΔG^0_{Ox} is the free energy of combustion as defined by Equation (1), and dn/dt describes the flow-dependent rate of the biomass combustion reaction. Because the conversion of chemical into electrochemical energy can theoretically be achieved with 100% efficiency, the power efficiency of the cell can significantly exceed that of a photovoltaic cell (Shockley–Queisser limit of ca. 34% for a 1.1 eV bandgap of the light absorber). The chemical free energy that is converted in the device is 'free' because the biomass in wastewater is available at no cost and because air is abundant. However, to allow comparison with literature, all the efficiencies reported below neglect the free energy term in Equation (2).

Of the light-assisted biomass fuel cells reported to date, all have efficiencies considerably below the Shockley–Queisser limit.[6] In one of the first devices, Kaneko (2006) and co-workers employed a Pt-air electrode and a TiO_2 photoelectrode in

[a] R. L. Chamousis, Prof. F. E. Osterloh
Department of Chemistry
University of California, Davis
One Shields Avenue, Davis, CA 95616 (USA)
Fax: (+1) 5307528995
E-mail: fosterloh@ucdavis.edu

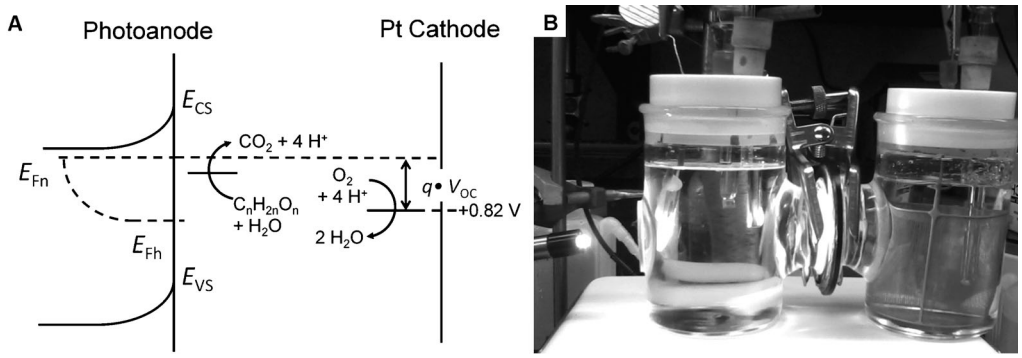

Figure 1. A) Energy scheme for the photoelectrochemical (PEC) solar cell containing a biomass photoanode and an oxygen counter-electrode. B) Photo of PEC reactor, showing photoanode compartment (left) and Pt/air electrode compartment (right).

the same compartment.[7] Under 500 W illumination from a Xe lamp, the device achieved up to 0.10 mW cm^{-2} electrical power (J_{SC} = 0.5 mA cm^{-2}, V_{OC} = 0.64 V, FF = 0.32) from aqueous 0.5 M glucose (containing 0.1 M Na_2SO_4), corresponding to 0.20 × 10^{-5}% photochemical energy conversion. The efficiency of the device under *solar* irradiation was not reported. Because the photoanode and cathode are located in one compartment, the performance of this device was probably limited by competing oxygen reduction at the photoanode (which leads to short-circuiting of the device). In 2011, Enright et al. published a cell that uses a TiO_2 photoanode in combination with an inexpensive MnO_2 air electrode for the oxidation of formic acid, 2-propanol, 1,2-dihydroxybenzene, and ascorbic acid.[8] Under sunlight, the device power output reached 31.5 mW m^{-2}, which is equivalent to 3.15 × 10^{-3}% solar conversion efficiency. This relatively low power output is partially a result of the greater oxygen reduction overpotential of MnO_2, compared to platinum.

Herein, we study the performance characteristics of two fuel cells containing either WO_3 or TiO_2 photoanodes. In contrast to the Kaneko cell, separate electrode compartments are used to prevent oxygen reduction at the photoanode (short-circuiting). The efficiencies of the devices are measured with electrolyte only, synthetic wastewater, or with aqueous glucose, under sunlight or artificial light, and as a function of illumination wavelength. The devices have the highest photochemical efficiencies reported to date, but their performance is still limited by mass transport, substrate concentration, and insufficient visible light absorption by the photoelectrodes. The high cost of the platinum cathode is also an issue for commercial applications of this technology.

Results and Discussion

The solar biomass fuel cell is shown in Figure 1B. The two-compartment cell employs a Pt electrode in the cathode compartment and TiO_2 or WO_3 film electrodes in the photoanode compartment. A quartz window allows entry of UV light into the cell. The TiO_2 and WO_3 films were synthesized based on published procedures on top of a fluorine-doped tin oxide (FTO) electrode.[9] The Aeroxide P25 TiO_2 contains anatase and rutile in a 4:1 ratio. The X-ray diffraction (XRD) pattern for WO_3 confirms the presence of monoclinic WO_3 (Figure 2).[10] The high intensity of the (002) plane indicates that preferred orientation occurs in the (001) plane. Scanning electron microscopy (SEM) images reveal that the WO_3 film consists of sheet-like particles over a range (0.2 to 0.5 μm) of sizes, with variable thicknesses averaging 23 ± 6 nm (Figure 3A). The TiO_2 film consists of 25 ± 5 nm particles, in accordance with the particle size in the precursor (Figure 3C). The average thicknesses of the WO_3 and TiO_2 films, as measured by SEM, are 3.5 μm and 17 μm, respectively (Figure 3B, D). The diffuse reflectance spectra reveal absorption edges of 407 nm and 468 nm for TiO_2 and WO_3, corresponding to band gaps of 3.05 eV and 2.65 eV (Figure 4).

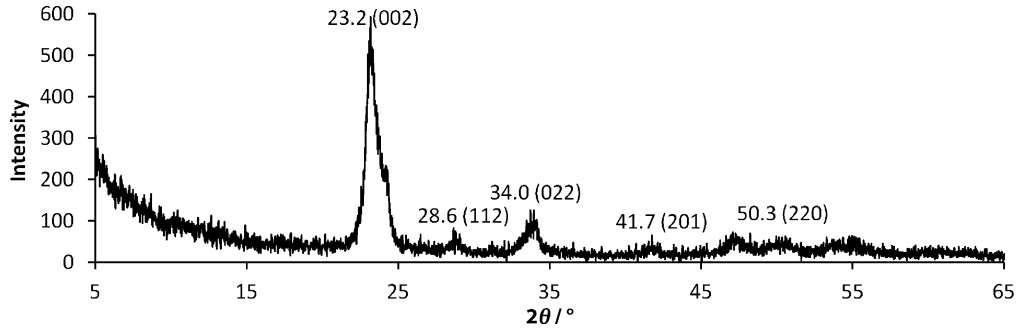

Figure 2. X-ray diffraction pattern for monoclinic WO_3 annealed at 500 °C with Bragg indices labeled.

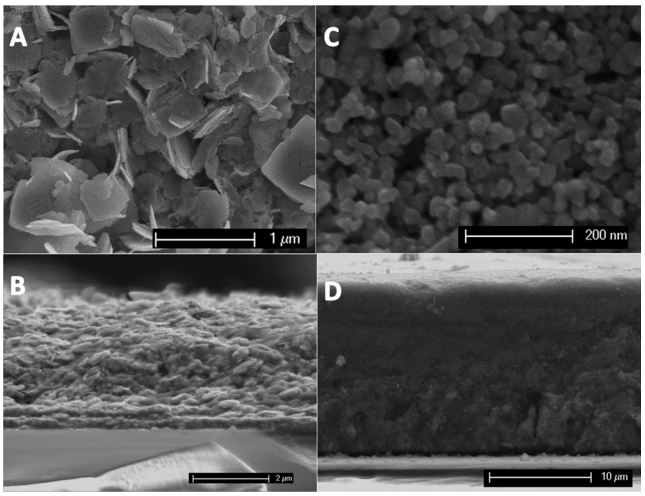

Figure 3. A) Front view, and B) side view scanning electron microscopy (SEM) images of WO_3 on FTO. c) Front view, and d) side view SEM images of TiO_2 on FTO.

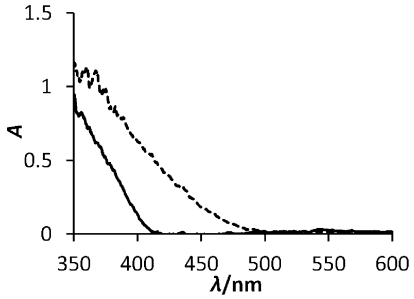

Figure 4. Scatter-corrected diffuse reflectance spectra for films on FTO. Solid line: TiO_2, dashed line: WO_3.

In order to study the energetics for glucose oxidation, electrochemical and photoelectrochemical experiments were performed on the TiO_2 and WO_3 electrodes. Cyclic voltammograms under dark conditions are shown in Figure 5. The solid curves show the anodic current for 0.1 M aqueous KCl, and the dashed curves for 0.1 M aqueous KCl containing 0.5 M glucose. For both electrodes, no significant current was observed below 1.5 V (NHE). Above 1.5 V, an anodic current formed due to water oxidation. The overpotential (measured at 1.0 mA cm^{-2}) is 1.10 V for the TiO_2 electrode and 1.16 V for the WO_3 electrode. Interestingly, the addition of glucose to the electrolyte does shift the oxidation potential to higher values (2.02 V for TiO_2 and 2.04 V for WO_3). This suggests that under these conditions water oxidation is preferred at the electrode. It is known from earlier studies that the glucose oxidation potential depends strongly on pH,[11] the electrode materials, and the electrolyte.[12] When electrochemical scans are repeated under chopped illumination, the situation is different (Figure 6). In the absence of glucose, photo-onset potentials in 0.1 M KCl occur at −0.32 V vs. NHE at for TiO_2 and at +0.30 V vs. NHE for WO_3. These values agree well with the published flatband potentials for these materials.[13] In both cases the photocurrent is due to water oxidation. When glucose is added to a 0.5 M final

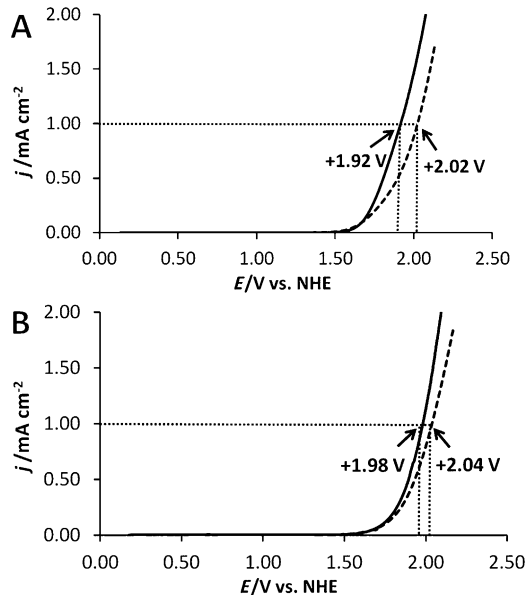

Figure 5. Dark oxidative scans for films on FTO: A) TiO_2 and B) WO_3 in (solid line) 0.1 M KCl at pH 7, and (dashed line) 0.1 M KCl and 0.5 M glucose at pH 7.

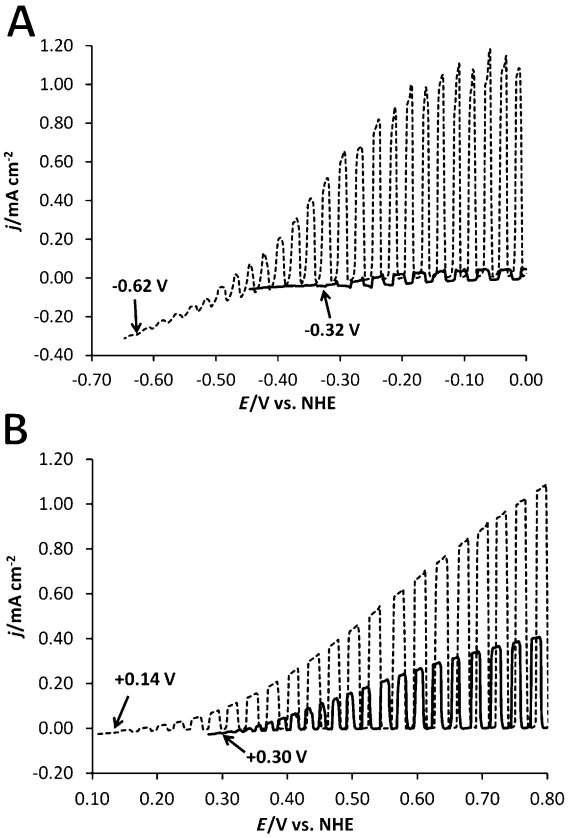

Figure 6. Photocurrent scan for A) TiO_2, and B) WO_3. Both on FTO using chopped light from 300 W Xe arc lamp in (solid line) 0.1 M KCl at pH 7, and (dashed line) 0.1 M KCl/0.5 M glucose at pH 7.

concentration, the current density doubles in the case of WO_3 and increases by a factor of 10 for TiO_2 (Figure 6 A and B). In addition, the photo-onset potentials shift to lower values (−0.62 V for TiO_2 and 0.14 V for WO_3). This clearly shows that

glucose is preferentially oxidized over water and becomes the main electron source under illumination. The shift in the photo-onset potential toward more negative values may be due to adsorption of glucose or of its oxidation products to the semiconductor electrodes. The dependence of the flatband potential of the semiconductor on adsorbates is well documented.[14]

In order to probe the wavelength dependence of the photoreaction, electrochemical scans were repeated under monochromatic irradiation, using a fixed applied potential of +0.8 V vs NHE (pH 7). To calculate incident photon to current conversion efficiencies (IPCE), the measured photocurrent densities

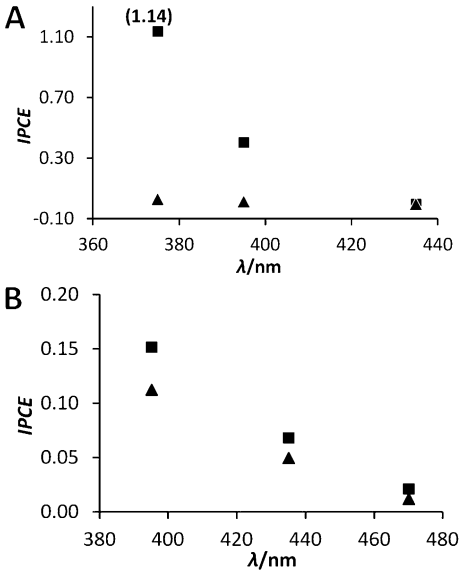

Figure 7. IPCE data curves for A) TiO_2, and B) WO_3 on FTO at 0.8 V vs NHE in (▲) 0.1 M KCl at pH 7, and (■) 0.1 M KCl/0.5 M glucose at pH 7.

were divided by the photon flux at each wavelength. Values with and without 0.5 M glucose are shown in Figure 7 as a function of the wavelength. For TiO_2, IPCE values are highest at 370 nm and decay with increasing wavelength to reach zero at 435 nm, in agreement with the 3.05 eV bandgap of the material. At 370 nm, the IPCE value exceeds unity, which shows that more than one electron is generated per photon. This is due to current doubling, that is, the generation of secondary electrons from unstable photo-oxidation intermediates. This effect has been previously observed for TiO_2 under similar conditions (0.5 M KCl, 5×10^{-3} M CH_3OH, pH 7).[15] Measurements in the absence of glucose lead to substantially lower IPCE values at all wavelengths. This confirms that glucose acts as the preferred redox species in the photoelectrochemical experiments. The IPCE curves for WO_3 are shown in Figure 7 B. Again, a trend of diminishing activity with increasing wavelength is observed. In contrast to TiO_2, WO_3 remains active in visible light, producing an IPCE value of 0.02 at 470 nm.

However, overall IPCE values for WO_3 are substantially lower than for TiO_2, which can be attributed to the lower thickness of the WO_3 film (3.5 μm compared to 17 μm for TiO_2). In addition, IPCE values depend less on the presence of glucose. This shows that WO_3 has a lower selectivity and lower activity for glucose oxidation than TiO_2.

To produce electricity in accordance with the scheme in Figure 1 A, the photoanodes were placed in series with a platinum air cathode that was located in a separate compartment of the electrochemical cell. The cathode consisted of a Pt mesh electrode immersed in an oxygen saturated 0.1 M KCl solution. A filter paper served as the ion bridge between both compartments. Power measurements for this configuration were recorded under solar irradiation, under monochromatic irradiation, and using either 0.5 M glucose/0.1 M KCl in the anode compartment, or synthetic wastewater. Illumination was performed through the electrolyte onto the photoactive film (not through the FTO electrode). The results are summarized in Table 1 for water, aqueous glucose, and synthetic wastewater. Net conversion of chemical and solar energy into electrical energy is observed in all cases.

The data for experiments in 0.5 M glucose solution reveals the following:

1. The open circuit voltage for TiO_2 is more than twice as high (≈1.15 V) as for WO_3 (≈0.50 V). This is due to the more negative flatband potential of TiO_2 (−0.2 V NHE) compared to WO_3 (+0.30 V NHE; see Figure 1 A).
2. The short circuit current for TiO_2 (3–4 mA) is 15–20 times higher than for WO_3 (≈0.2 mA) in agreement with the measured higher photochemical activity of this electrode.

Table 1. Electrical power output for continuously illuminated TiO_2 and WO_3 photoelectrodes connected to a Pt-air counterelectrode. Data is for water, 0.5 M glucose, or synthetic wastewater (SWW). The pH was 7 in all cases, and 0.1 M KCl was present for the measurements in glucose and water. The cathode and anode compartments were purged with O_2 and N_2, respectively, before measurement.

Anode	Illumination wavelength [nm]	Intensity [W cm^{-2}]	V_{OC} [V]	I_{SC} [A cm^{-2}]	*FF*	*P* [W cm^{-2}]	η [%]
TiO_2 (water)	395	0.043	0.87	2.7×10^{-4}	0.50	1.2×10^{-4}	0.27
WO_3 (water)	435	0.027	0.38	7.9×10^{-5}	0.14	4.2×10^{-6}	0.02
TiO_2 (water)	sunlight	0.100	0.88	2.2×10^{-4}	0.50[a]	9.7×10^{-5}	0.09
WO_3 (water)	sunlight	0.100	0.30	1.8×10^{-4}	0.14[a]	7.6×10^{-6}	0.01
TiO_2 (glucose)	395	0.043	1.13	4.3×10^{-3}	0.15	7.3×10^{-4}	1.7
WO_3 (glucose)	435	0.025	0.51	1.7×10^{-4}	0.16	1.4×10^{-5}	0.05
TiO_2 (glucose)	sunlight	0.100	1.15	3.3×10^{-3}	0.15[a]	5.7×10^{-4}	0.56
WO_3 (glucose)	sunlight	0.100	0.45	2.0×10^{-4}	0.16[a]	1.4×10^{-5}	0.01
TiO_2 (SWW)	395	0.043	0.75	9.2×10^{-5}	0.38	2.6×10^{-5}	0.06
WO_3 (SWW)	435	0.027	0.65	8.5×10^{-5}	0.18	1.0×10^{-5}	0.04
TiO_2 (SWW)	sunlight	0.100	0.90	1.7×10^{-4}	0.38[a]	5.8×10^{-5}	0.06
WO_3 (SWW)	sunlight	0.100	0.49	1.4×10^{-4}	0.18[a]	1.2×10^{-5}	0.01

[a] Estimated, based on 395/435 nm irradiations with 0.1 M KCl or 0.1 M KCl/0.5 M glucose.

3. Fill factors are equally low (0.15) for WO_3 and TiO_2. This is likely a result of mass and charge transport limitations across the cell.
4. Overall, the electrical power output for TiO_2 ($\approx$0.7 mW) is forty to fifty times above that of WO_3 ($\approx$0.01 mW). Correspondingly, the photochemical energy conversion efficiency of the TiO_2 electrode (1.7% under 395 nm illumination) was higher than that of the WO_3 electrode (0.05% under 435 nm illumination). When actual sunlight is used, the efficiency decreases by a factor of 3–5 since the intensity of the entire spectrum, including the non-absorbed part, is factored into the calculation.

In water (with 0.1 M KCl), the performance trends regarding WO_3 and TiO_2 are similar, but overall electrical output of the cell is diminished due to the higher overpotentials for water oxidation, compared to glucose, and to the increase of the flatband potentials for the photoelectrode materials. These factors lead to a reduction of the open circuit voltage of the device and a reduction of the photocurrent. Overall, WO_3 is less affected by this performance reduction because of its ability to oxidize water directly—the efficiency for WO_3 drops by a factor of two only, whereas that of TiO_2 is diminished by a factor of six.

For the WO_3 device, the situation with synthetic wastewater is intermediate between the water and glucose experiments. This shows that the reduced substrate concentration (SWW only contains 0.00076 M of glucose) is the main factor for the lower performance. However, for the TiO_2 device, the output with SWW is actually lower (e.g., 0.06% with 395 nm light) than that with water (e.g., 0.27% with 395 nm light). This indicates that other effects (e.g., HPO_4^{2-}, Ca^{2+}, Na^+ ion adsorption to the photoelectrode) must play a role for this material.

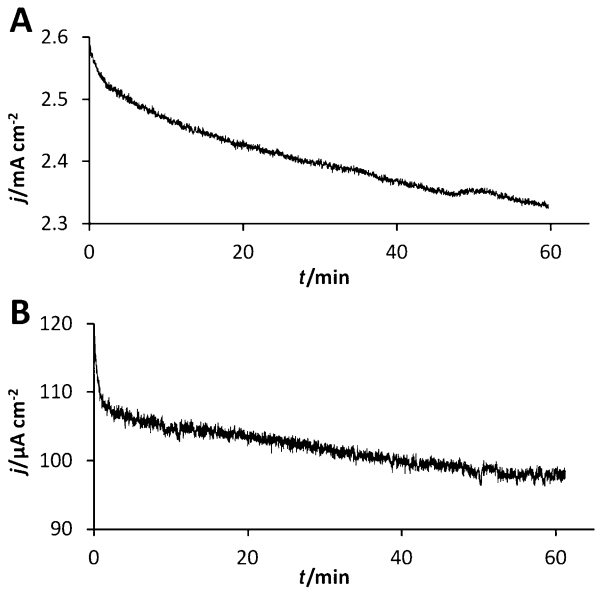

Figure 8. Long-term irradiation test using A) TiO_2, and B) WO_3 as photoanode in 0.1 M KCl/0.5 M glucose at pH 7 connected to Pt-air counterelectrode in 0.1 M KCl at pH 7. Illumination: 16 mW cm^{-2} of 395 nm for TiO_2 or 35 mW cm^{-2} of 435 nm light for WO_3.

Finally, to test continuous performance of the devices, a 60 min irradiation test was conducted for both photoelectrodes in 0.5 M glucose/0.1 M KCl solution at pH 7 (Figure 8). Over this timeframe, the TiO_2 and WO_3 both show a decrease in current density, equivalent to a reduction of performances of 10 and 20% for each material, respectively. The decay is at least partially due to depletion of glucose in the electrolyte solution, but other factors (e.g. electrode degradation) may also be important, although no adsorption of organic substrate or film instability was visibly observed.

Conclusions

We demonstrate electrical power generation by WO_3- and TiO_2-based solar biomass fuel cells under solar and artificial light. The power of these devices depends strongly on the electrode material and illumination and can reach up to 0.73 mW cm^{-2}, equivalent to three times the performance of microbial fuel cells.[1a,2] The measured efficiency of 1.7% for TiO_2 exceeded the values previously reported in the literature.[7,8] However, the performance of the cells remains significantly below the Shockley–Queisser limit. This is in part due to the low fill factors, which result from sub-optimal device geometry leading to high transport resistance. Even though higher efficiencies could be obtained in solutions of higher pH (where metal oxide photocatalysts perform better), solutions of pH 7–8 were required to test the practicality of using these photocatalysts in an actual wastewater treatment plant. Furthermore, a significant optimization should be possible by bringing the electrodes closer together and by matching the thickness of the films with their light absorption. More difficult will be to increase the photoresponse of the electrode materials, especially in visible light. And, as the results for synthetic wastewater show, low substrate concentrations and extraneous ions can further reduce power output. To overcome these problems will require new electrode materials with greater activity and stability and also a substitute for the expensive platinum counter-electrode.

Experimental Section

Reagents: Sodium tungstate (99% A.C.S. purity), Triton X-100, and D-(+)-glucose (ACS reagent) were purchased from Sigma–Aldrich. Aeroxide P25 titanium dioxide (99.0% purity) was purchased from Acros Organics. Potassium chloride (99% purity), sodium phosphate dibasic heptahydrate (98% purity), and magnesium sulfate anhydrous (98% purity) were purchased from EM Science. Calcium chloride dihydrate (99% purity) and sodium chloride (99% purity) were purchased from EMD Chemicals. Potassium sulfate (99% purity) was purchased from Mallinckrodt. Potassium hydroxide (87.2% purity) and hydrochloric acid (37.3% purity) were purchased from Fischer Scientific. The platinum counterelectrode was purchased from Heraeus Metal Processing, LLC. Water was purified by a Nanopure II system to a resistivity of $>$18 MΩ cm. Solutions were sparged with high-purity nitrogen gas (99.9%).

WO_3: The precursor tungstic acid solution was synthesized according to a published procedure.[9a] A 0.5 M sodium tungstate ($Na_2WO_4 \cdot 2H_2O$) solution was passed through a protonated Dowex

50W-X8 ion exchange column. The yellow effluent was collected and aged with constant stirring for 3 days. This precursor solution was used within 2 weeks to produce WO_3 films by drop-coating the tungstic acid solution onto FTO-coated glass electrodes and annealing at 500 °C for 30 min.

TiO_2: Aeroxide P25 TiO_2 nanoparticles (250 mg, 3.1 mmol) were ground by mortar and pestle and dispersed in 0.375 mL water. The slurry was sonicated for 15 min. A drop of Triton X-100 was added to the mixture and sonicated for another 15 min. The white paste was used to produce TiO_2 films by doctor-blading the paste onto FTO-coated glass electrodes and annealing at 500 °C for 30 min.

Synthetic wastewater: A solution of synthetic wastewater was prepared based on a published procedure.[16] The mixture consisted of glucose (0.134 g, 0.7 mmol), urea (0.05 g, 0.8 mmol), $Na_2HPO_4{\cdot}2H_2O$ (0.186 g, 1.3 mmol), $CaCl_2{\cdot}2H_2O$ (0.188 g, 1.3 mmol), NaCl (0.03 g, 0.5 mmol), KCl (0.014 g, 0.2 mmol), and $MgSO_4$ (0.01 g, 0.1 mmol) per liter of water, equivalent to 250 mg L^{-1} chemical oxygen demand (COD). The pH of the solution was 7.6.

Instruments: XRD patterns were obtained by using a Scintag XDS2000 powder X-ray diffractometer with monochromatic Cu K_α radiation. The WO_3 sample was prepared by drying a thin film of the annealed WO_3 suspended in ethanol onto a zero-diffraction Si plate. SEM measurements were performed on a FEI XL30-SFEG high-resolution scanning electron microscope operating at 5 kV. The samples were prepared by cutting a 0.5 cm^2 area of the electrode using a diamond saw. The edge to be imaged was gently sanded before placing into the SEM. Diffuse reflectance spectra were obtained on powders calcined at 500 °C using an Ocean Optics HR2000 CG-UVNIR spectrometer with a DH2000 light source. All spectra were scatter-corrected by applying a least-squares fit to a part of the spectrum where the absorbance was only caused by scattering. This calculated scatter contribution was applied to all wavelengths, and these new values were subtracted from the measured absorbance values, resulting in a scatter-corrected plot.

Electrochemical measurements were performed using a three-electrode cell equipped with a Pt counterelectrode and SCE reference electrode. A fluorine-doped tin oxide (FTO) coated glass electrode (1.0 cm^2 exposed area) served as the working electrode. Films of WO_3 and TiO_2 were deposited on the electrode by doctor-blading and annealing at 500 °C for 30 min. Electrochemical measurements were conducted in aqueous 0.1 M KCl or 0.5 M glucose/0.1 M KCl at pH 7. The solutions were degassed with N_2 for ten minutes prior to each measurement. The potential of the $K_4[Fe(CN)_6]$ redox couple (+0.36 V vs NHE) was used to calibrate each measurement. Potentials were generated and currents observed with a Gamry Reference 600 potentiostat controlled by a PC. Dark voltammograms were produced by applying anodic scans (10 mV s^{-1}). Photocurrent onset potentials were determined by applying cathodic scans (10 mV s^{-1}) with chopped light from a 300 W Xe arc lamp, filtered with a water IR filter, and directed onto the working electrode using SiO_2 fiber optics. The power at the electrode was 100 ± 20 mW cm^{-2} as measured with a GaAsP photodetector (280–660 nm sensitivity range). Light for incident photon to charge carrier efficiency calculations were produced by Roithner LEDs of 375 nm (2.0 mW cm^{-2}), 395 nm (14.5 mW cm^{-2}), 435 nm (14.5 mW cm^{-2}), and 470 nm (70.0 mW cm^{-2}) light. The power at the electrode in each case was measured with an International Light Technologies GaAsP photodetector and adjusted for the sensitivity of the detector at different wavelengths.

Electrical power measurements were conducted with the two chamber PEC reactors shown in Figure 1 B. It was filled with either 0.1 M KCl (pH 7), 0.5 M glucose/0.1 M KCl (pH 7), or synthetic wastewater (pH 7.6) in the anode compartment under constant stirring. The cathode compartment contained a Pt counterelectrode in either O_2-saturated 0.1 M KCl (pH 7) or synthetic wastewater (pH 7.6). The two compartments were separated when appropriate with a Whatman paper membrane. Sunlight was collected at 12 noon in Davis, California (38.54°, −121.75°). Monochromatic light was generated as described above.

Acknowledgements

This work was supported by the California Energy Commission (56395A/09–06) and by the National Science Foundation under grants 0829142 and 1133099.

Keywords: biomass · fuel cells · photocatalysis · photoelectrochemical cell · solar energy

[1] a) H. Liu, R. Ramnarayanan, B. E. Logan, *Environ. Sci. Technol.* **2004**, *38*, 2281; b) W. Rulkens, *Energy Fuels* **2008**, *22*, 9; c) A. J. Frank, N. Kopidakis, J. v. d. Lagemaat, *Coord. Chem. Rev.* **2004**, *248*, 1165.

[2] T. Catal, S. Xu, K. Li, H. Bermek, H. Liu, *Biosens. Bioelectron.* **2008**, *24*, 849.

[3] H. Gerischer, *J. Electroanal. Chem.* **1975**, *58*, 263.

[4] K. F. Honda, *Bull. Chem. Soc. Jpn.* **1971**, *44*, 1148.

[5] D. Laser, A. J. Bard, *J. Electrochem. Soc.* **1976**, *123*, 1027.

[6] a) R. Solarska, C. Santato, C. Jorand-Sartoretti, M. Ulmann, J. Augustynski, *J. Appl. Electrochem.* **2005**, *35*, 715; b) X. Z. Li, H. S. Liu, *Environ. Sci. Technol.* **2005**, *39*, 4614; c) M. Antoniadou, D. I. Kondarides, D. Labou, S. Neophytides, P. Lianos, *Sol. Energy Mater. Sol. Cells* **2010**, *94*, 592; d) M. Kaneko, H. Ueno, K. Ohnuki, M. Horikawa, R. Saito, J. Nernoto, *Biosens. Bioelectron.* **2007**, *23*, 140; e) M. Kaneko, H. Ueno, R. Saito, S. Suzuki, J. Nemoto, Y. Fujii, *J. Photochem. Photobiol. A* **2009**, *205*, 168; f) P. Lianos, *J. Hazard. Mater.* **2011**, *185*, 575.

[7] a) M. Kaneko, J. Nemoto, H. Ueno, N. Gokan, K. Ohnuki, M. Horikawa, R. Saito, T. Shibata, *Electrochem. Commun.* **2006**, *8*, 336; b) H. Ueno, J. Nemoto, K. Ohnuki, M. Horikawa, M. Hoshino, M. Kaneko, *J. Appl. Electrochem.* **2009**, *39*, 1897.

[8] P. Enright, A. Betts, J. Cassidy, *J. Appl. Electrochem.* **2011**, *41*, 345.

[9] a) A. Chemseddine, R. Morineau, J. Livage, *Solid State Ionics* **1983**, *9–10*, 357; b) M. K. Nazeeruddin, A. Kay, I. Rodicio, R. Humphry-Baker, E. Mueller, P. Liska, N. Vlachopoulos, M. Grätzel, *J. Am. Chem. Soc.* **1993**, *115*, 6382.

[10] a) Y.-G. Choi, G. Sakai, K. Shimanoe, N. Miura, N. Yamazoe, *Sens. Actuators B* **2002**, *87*, 63; b) J. Augustynski, C. Santato, M. Odziemkowski, M. Ulmann, *J. Am. Chem. Soc.* **2001**, *123*, 10639.

[11] F. Largeaud, K. B. Kokoh, B. Beden, C. Lamy, *J. Electrochem. Soc.* **1995**, *397*, 261.

[12] M. W. Hsiao, R. R. Adzic, E. B. Yeager, *Electrochim. Acta* **1992**, *37*, 357.

[13] a) M. T. Nenadovic, T. Rajh, O. I. Micic, A. J. Nozik, *J. Phys. Chem.* **1984**, *88*, 5827; b) A. Fujishima, X. Zhang, D. A. Tryk, *Surf. Sci. Rep.* **2008**, *63*, 515.

[14] a) D. S. Ginley, M. A. Butler, *J. Electrochem. Soc.* **1978**, *125*, 1968; b) P. Singh, R. Singh, R. Gale, K. Rajeshwar, J. DuBow, *J. Appl. Phys.* **1980**, *51*, 6286.

[15] a) S. T. Martin, H. Herrmann, M. R. Hoffmann, *J. Chem. Soc. Faraday Trans.* **1994**, *90*, 3323; b) J. Anthony Byrne, B. R. Eggins, P. S. M. Dunlop, S. Linquette-Mailley, *Analyst* **1998**, *123*, 2007.

[16] Y. S. Park, J. W. Yun, D. S. Kim, S. K. Song, *Biotechnol. Tech.* **1998**, *12*, 459.

Received: January 8, 2012
Published online on April 23, 2012

